Available online at www.sciencedirect.com

SCIENCE DIRECT®

Journal of Nuclear Materials 351 (2006) 285–294

journal of nuclear materials

www.elsevier.com/locate/jnucmat

Destruction processes of large stacking fault tetrahedra induced by direct interaction with gliding dislocations

Y. Matsukawa *, Yu.N. Osetsky, R.E. Stoller, S.J. Zinkle

Metals and Ceramics Division, Oak Ridge National Laboratory, P.O. Box 2008, MS-6138, Oak Ridge, TN 37831-6138, USA

Abstract

The destruction process of large non-truncated stacking fault tetrahedra (SFTs) induced by gliding dislocations was examined by in situ transmission electron microscope straining experiments. Three different destruction processes were observed: a triangular Frank loop remained after the collapse (Type 1), the whole SFT was incorporated into a gliding dislocation as multiple super jog segments (Type 2), and an apex portion of the original SFT remained as a smaller SFT while the base portion was annihilated (Type 3). The remnants of Type 1 and 2 destruction processes were similar to those of previous models proposed by Kimura, indicating that these processes are based on dislocation reactions as assumed in Kimura models. On contrary, the Type 3 process, which was entirely different from Kimura models, is occasionally accompanied by vacancy migration.

---

1. Introduction

Defect clusters introduced by high-energy particle irradiation are obstacles for dislocation glide, causing material hardening on a macroscopic scale. Concurrently, the hardened materials often lose ductility, indicating that the ductility reduction is also related to the defect clusters. Local defect-free bands are frequently observed in the deformation microstructure of irradiated specimens [1–5]. Once the defect-free bands are created, subsequent deformation localizes in these bands because they are favorable sites for dislocation glide due to the absence of defect cluster hardening barriers. As a result of flow localization on a microscopic scale, materials lose their ductility on a macroscopic scale. Considerable research has been directed to understanding the formation mechanism of localized defect-free bands, and associated dislocation channeling [1–6]. The physical process of cleared channel formation is destruction and/or annihilation of defect clusters by gliding dislocations. Although various types of defect clusters can be introduced by irradiation, stacking fault tetrahedra (SFTs) are of particular interest in nuclear materials research. This is because SFTs are the predominant vacancy cluster morphology in many neutron irradiated fcc metals [7–9]. Computer simulations using molecular dynamics (MD) codes have indicated that SFTs are directly produced by cascade damage during neutron irradiation of fcc metals such as copper that

---

* Corresponding author. Tel.: +1 865 241 3650; fax: +1 865 574 0641.

E-mail address: matsukaway@ornl.gov (Y. Matsukawa).

0022-3115/$ - see front matter © 2006 Elsevier B.V. All rights reserved.
doi:10.1016/j.jnucmat.2006.02.003

have a low stacking fault energy [10]. However, the physical mechanisms involved in SFT-dislocation interaction still remains unclear. This is mainly due to the complicated crystallographic geometry of the SFT. Since several types of interaction are conceivable, it is difficult to specify which process really takes place by theory alone.

It is well known that dislocation channeling occurs in quenched metals containing SFTs [11,12] and vacancy loops [13] as well as irradiated metals. In the present paper, we summarize the SFT destruction processes observed by in situ transmission electron microscope (TEM) straining experiments using quenched gold containing relatively large SFTs.

2. Experimental procedure

SFTs were introduced into 99.9975% purity polycrystalline gold specimens, whose thickness was 100 μm, by quenching from 1273 K in an open vertical furnace to 233 K in $CaCl_2$ solution. Since vacancies are mobile at room temperature in gold, the formation behavior of SFT is sensitive to the thermal history after quenching [14]. The specimens were kept at 233 K for 1 h, then at 298 K for 2 h, and finally at 373 K for 1 h, before electro-polishing. This quenching and aging treatment produced large (average edge length of ~45 nm) perfectly formed SFTs with no observable tetrahedron-truncation. Tensile specimens for in situ straining experiments had a rectangular shape (10 mm × 2.5 mm × 100 μm). The central portion was electro-polished by the twin jet method. The electrolyte polishing solution was KCN 67 g/l water solution, and the polishing temperature was 276 K. in situ straining experiments were carried out at both room temperature and 100 K. The accelerating voltage of TEM was 200 kV, which does not introduce any irradiation damage into gold. The crosshead speed of the straining stage was 0.1 μm/s.

3. Results

SFT destruction was induced by direct interaction with gliding dislocations. The processes frequently observed were categorized in terms of the remnants remaining after the destruction of SFT.

The first SFT destruction process (Type 1) leaves a triangular Frank loop behind, as shown in Fig. 1. In this figure the beam direction was close to $\langle 0\,0\,1\rangle$; the SFT is visible as a nearly square image in this orientation. The position of the remnant triangular Frank loop corresponded to one of the four stacking faults comprising the original SFT. This collapse process is essentially the inverse reaction of the Silcox-Hirsch mechanism, which was originally proposed as a formation mechanism of an SFT based on dislocation reactions [15]. No jogged segments were formed on the dislocation that collapsed the SFT. Also, it is noteworthy that subsequent dislocations did not interact with the triangular Frank loop. The glide planes of these dislocations were parallel to the first dislocation that collapsed the SFT. Therefore, it is reasonable to conclude that the Frank loop was formed on a plane parallel to the glide plane of the dislocation that collapsed the SFT and did not interact with the subsequent dislocations gliding on parallel planes.

The second process (Type 2) leaves no remnants behind, as shown in Fig. 2. The vacancies comprising the SFT were incorporated into the impinging dislocation by forming multiple super jog segments on the dislocation. The location of the super jog segments corresponded to the edges of the original SFT.

The results shown in Figs. 1 and 2 were obtained at room temperature. Fig. 3(a) and (b) show the Type 1 and 2 processes, respectively during deformation at 100 K. These two processes were observed in the same grain. The SFTs in Fig. 3(a) and (b) corresponded to two different types of crystallographically equivalent SFTs. The dislocations that interacted with these two SFTs were generated from the same source, indicating that those dislocations had the same Burgers vector. These results indicate that the SFT-dislocation interaction is different depending on SFT geometry, i.e., whether apex up or down.

The third process (Type 3) leaves a smaller SFT behind, as shown in Figs. 4 and 5. In the Type 3 process, the small remnant SFT corresponds to the apex of the original SFT whereas the base portion of the SFT disappeared. The plane dividing the original SFT into two pieces corresponded to the glide plane of the dislocation that destroyed the SFT (Figs. 4 and 5) or the glide plane of a dislocation that interacted with the SFT prior to the dislocation that finally destroyed the SFT (Figs. 6 and 7) [16]. There were two variants in the Type 3 process, distinguished by whether or not a cluster of defects formed on the impinging dislocation. The first variant is shown in Fig. 4, where the dislocation cross-slipped on one face of the SFT and the

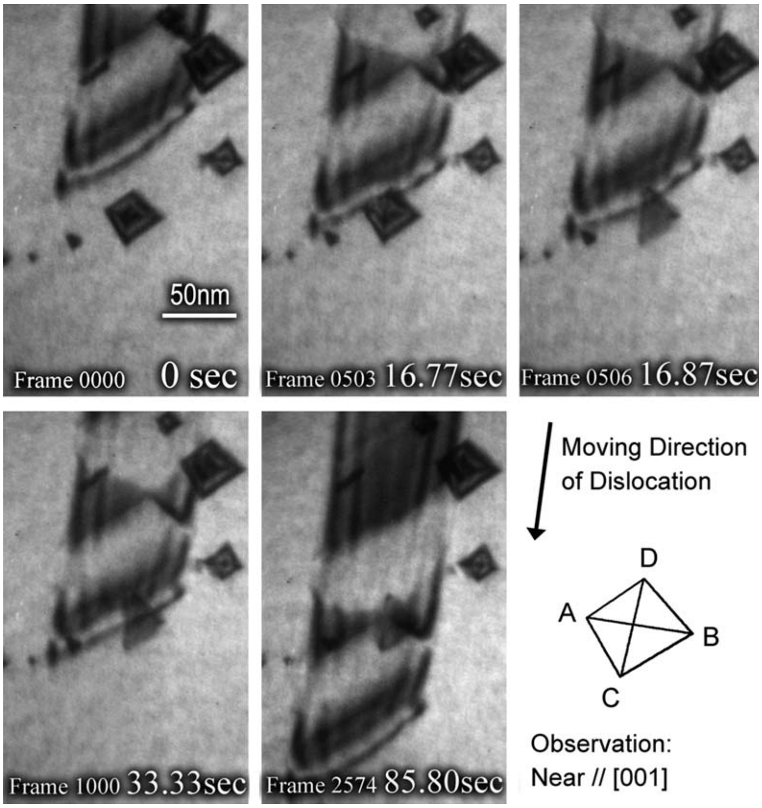

Fig. 1. Example of Type 1 SFT collapse process observed at room temperature. A triangular Frank loop remained behind following the collapse. The initial SFT size was 42 nm. The Thompson tetrahedron orientation of the SFT is also shown.

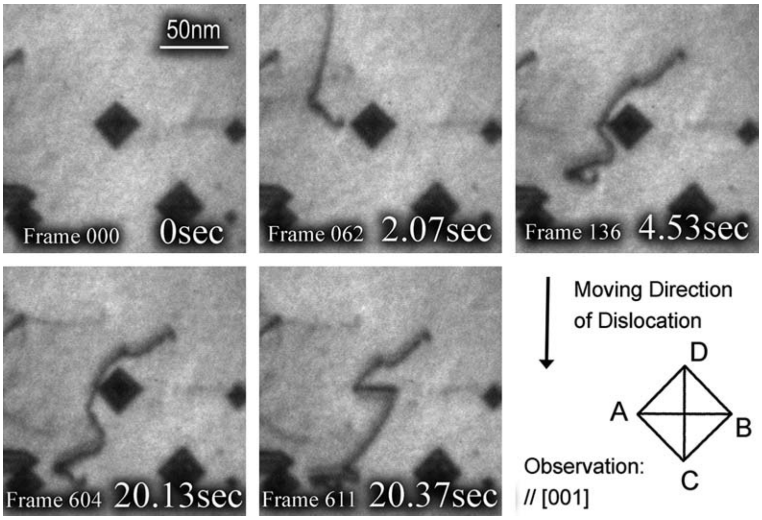

Fig. 2. Example of Type 2 SFT collapse process observed at room temperature. The whole SFT was incorporated the gliding dislocation as multiple super jog segments on it. The initial SFT size was 46 nm.

base portion of SFT disappeared (Frame 0803). The detailed geometry of this variant is shown in Fig. 5.

The second variant is shown in Fig. 6. In this case it is unclear whether the dislocation cross-slipped on

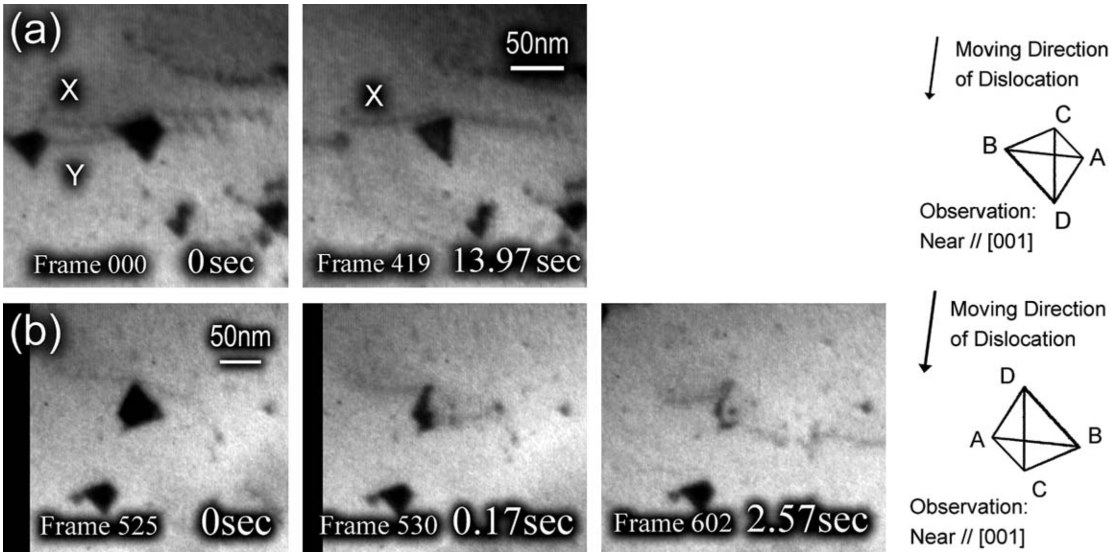

Fig. 3. Type 1 and 2 SFT collapse processes observed in the same grain at 100 K. (a) Type 1 process. Dislocation 'Y' collapsed the SFT when released from it. The initial SFT size was 47 nm. (b) Type 2 process. The initial SFT size was 55 nm.

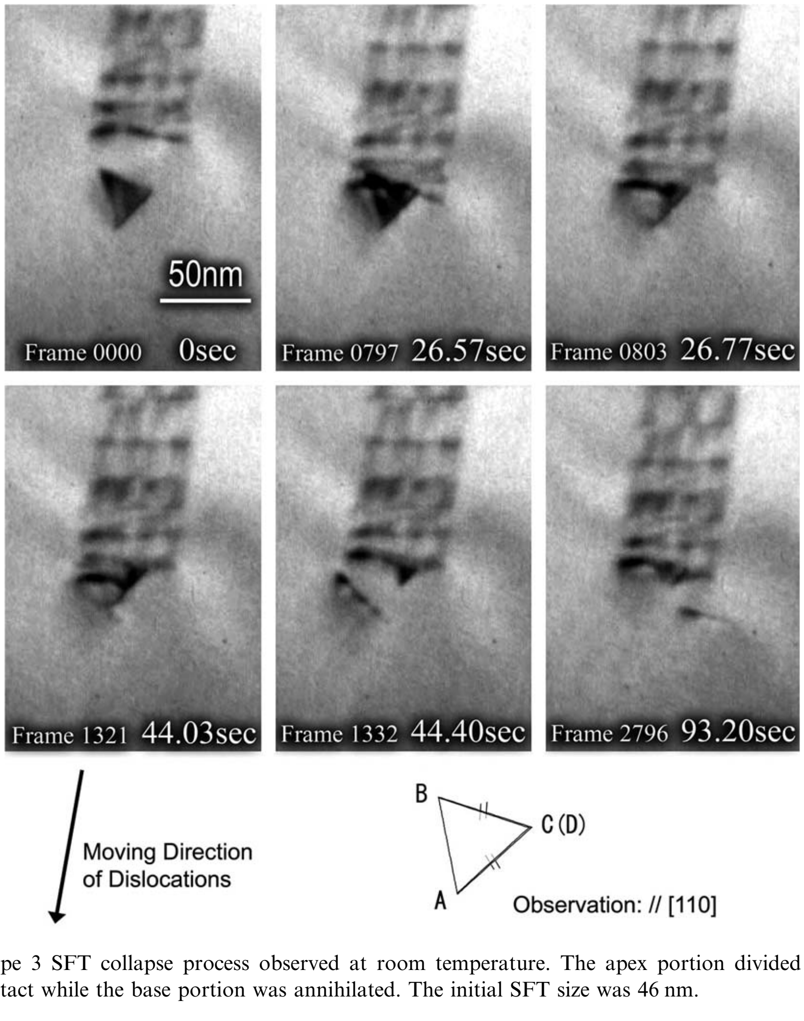

Fig. 4. Example of Type 3 SFT collapse process observed at room temperature. The apex portion divided by the gliding plane of dislocation remained intact while the base portion was annihilated. The initial SFT size was 46 nm.

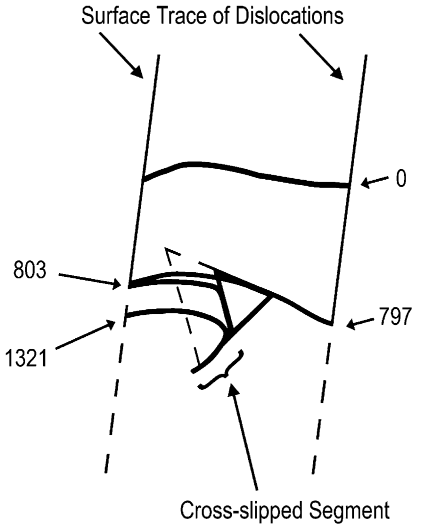

Fig. 5. Locus of the dislocation located at the forefront of pile-up. One of two ends of dislocation line intersected by specimen surfaces moved away from the trace of previous locus upon interaction, indicating that the dislocation cross-slipped on the SFT.

the SFT or cut through it. However, a cluster of defects formed on the dislocation in a location distinctly separated from the residual apex portion of the SFT when the base portion disappeared (Frame 3850) [16]. The detailed geometry of this variant is shown in Fig. 7. As the dislocation bowed out with increasing time and applied stress following the SFT interaction event, the cluster size gradually decreases, and a straight segment was developed on the dislocation. Considering that the SFT is a vacancy cluster, it would be reasonable to assume that this remnant is a vacancy cluster produced by re-aggregation of the vacancies formerly contained in the base portion of the original SFT.

4. Discussion

4.1. Comparison of the experimental conditions of the present in situ straining experiments with previous work using bulk specimens

The SFT sizes in the present in situ straining experiments are comparable to those in Yoshida's deformation study using quenched bulk gold [12] in terms of their stability. According to the numerical calculation by Jøssang and Hirth [17], SFTs in these two studies are both in the meta-stable size range, which is larger than 26.5 nm for gold. It is difficult to derive a definitive value for the localized strain rate in in situ TEM straining experiments due to microscopic heterogeneities of deformation associated with the irregular specimen shape. However, we can make a rough estimate of the strain rate from the motion of individual dislocations captured in the TEM movie. In the present dynamic observation dislocations glided intermittently; however, when they glided smoothly, the gliding distance was roughly 10^{-8}–10^{-7} m/s. This is very low speed deformation compared with MD simulations, in which the velocity of dislocation is commonly about 10^{1}–10^{3} m/s [18,19]. Assuming the dislocation density in the present TEM experiments is the same as the MD simulations (about 10^{14}–10^{15} m^{-2} [18]), the strain rate is roughly 10^{6}–10^{8} /s for MD [19], and 10^{-3}–10^{-2} /s for the present TEM experiments. As an alternative way, we can estimate the strain rate of in situ straining experiments from the cross-head speed of straining stage, 0.1 μm/s. The specimens were rectangular shape whose central portion was electro-polished by twin jet method. The diameter of the electro-polished portion is roughly 20 mm. The deformation should concentrate on the electro-polished portion due to the thickness difference. The thickness of electro-polished portion continuously changes; the thinnest is the central portion where a hole is present. The strain rate depends on what we consider the gauge length, i.e., over what portion of the overall specimen length is the deformation–concentrated zone. For example, assuming the gauge length is 10 mm, the strain rate is given as 10^{-5}/s. If the effective gauge length is 10 μm, the strain rate is 10^{-2}/s. The strain rate determined from the velocity of individual dislocation motion, 10^{-3}–10^{-2}/s, corresponds to the effective gauge length of 100–10 μm in the evaluation method using the crosshead speed. The width of thin foil portion transparent by 200 keV TEM (i.e., where deformation was actually occurring) was normally within this size range. Therefore, the strain rate of 10^{-3}–10^{-2}/s is a reasonable value for the present TEM experiments. Judging from the deformation temperature and the strain rate discussed here, the present in situ straining at room temperature is located in the range where dislocation channeling occurred in Yoshida's study [12], as shown in Fig. 8. Conversely, the in situ straining at 100 K is located in the range where channeling did not occur in Yoshida's study. Although we observed SFT collapse and annihilation even at 100 K, where channeling was not observed in Yoshida's study, our observation does

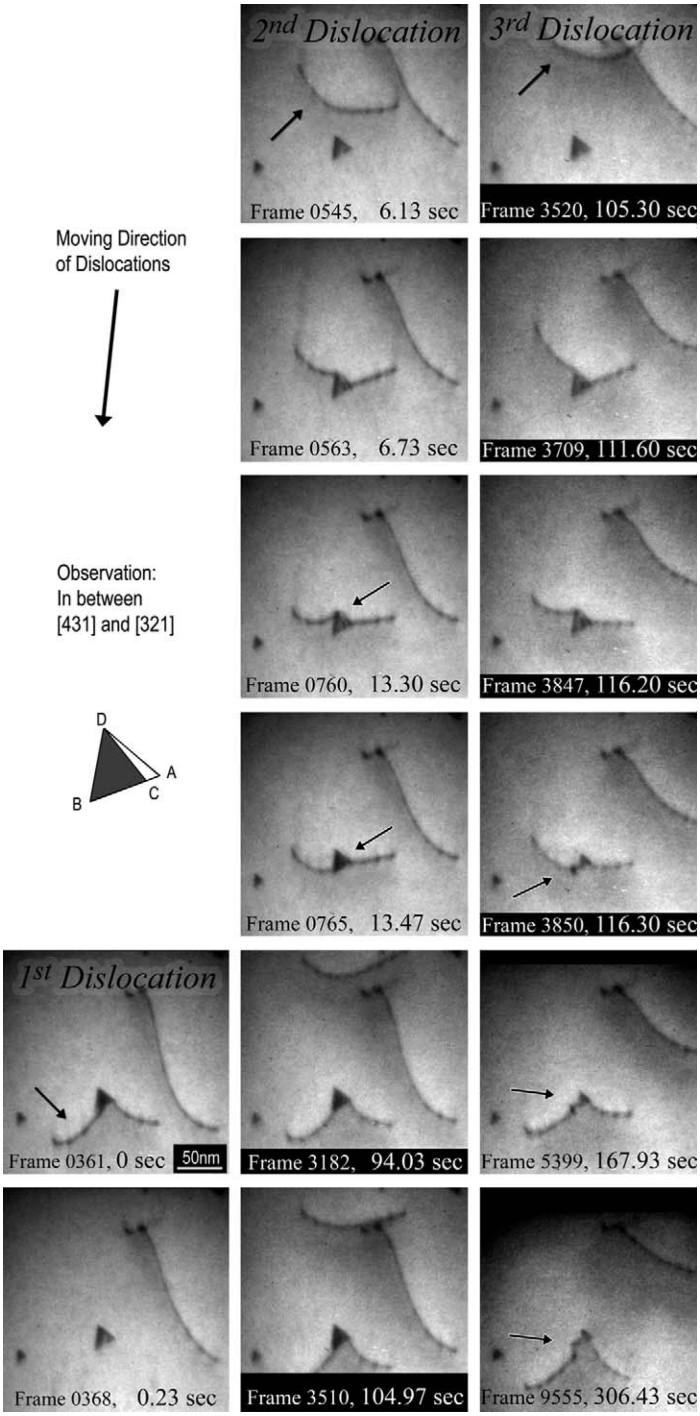

Fig. 6. Another example of Type 3 SFT collapse process observed at room temperature. The apex portion remained intact while the base portion was annihilated as well as Fig. 4. In addition to the remaining apex portion, there is another remnant formed on the dislocation at the moment of collapse (frame 3850). The initial SFT size was 27 nm.

not conflict with Yoshida's study. An important conclusion derived from these two results is that dislocations can annihilate SFTs even at 100 K; however, flow localization leading to cleared channel

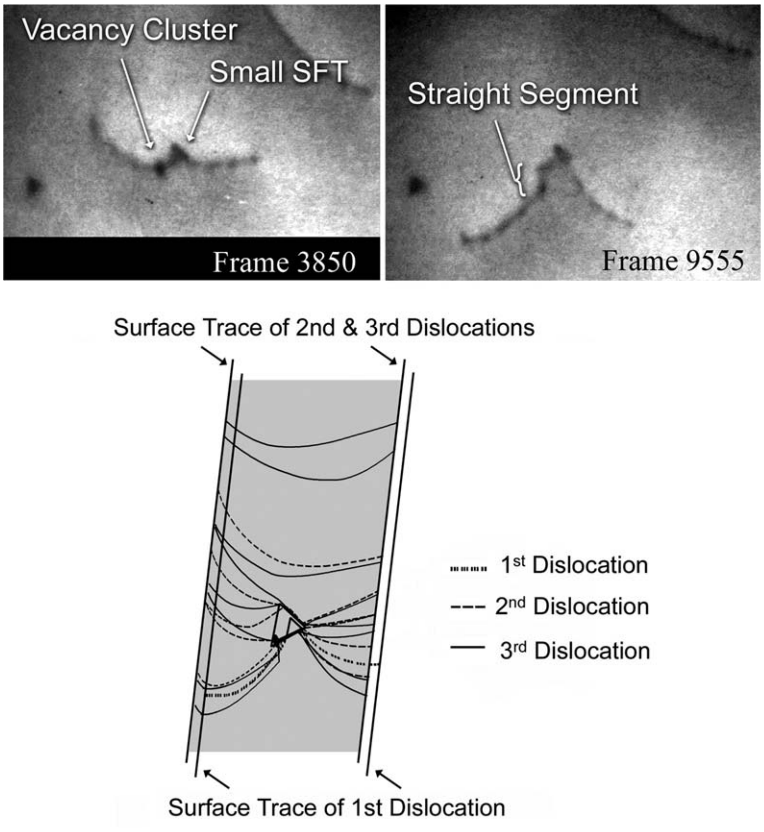

Fig. 7. Comparison of the locus of dislocations intersected the SFT. The locus analysis enables to make rough estimation about the glide plane of those dislocations and three-dimensional position of interaction on the SFT. The second and the third dislocations were gliding on almost identical plane. The smaller SFT left behind after the collapse of the original SFT corresponded to the apex portion divided by the gliding plane of the first dislocation, which was gliding closer to the apex than the following two dislocations.

formation does not occur in gold containing large SFTs at low temperature.

4.2. Comparison of the observed three SFT destruction processes with previous models

The Type 1 and 2 processes are quite similar to the SFT collapse models previously proposed by Kimura et al. [20]. Kimura analyzed how SFT can be collapsed by direct interaction with a gliding dislocation on the basis of dislocation reactions. The remnants remaining after the Type 1 and Type 2 processes resemble the remnants of Kimura's model for 60° mixed dislocation and screw dislocation, respectively. The results shown in Fig. 3 also support the idea that Type 1 and 2 processes are based on dislocation reactions as assumed in Kimura's two models [20]. As clearly seen in Fig. 6, the impinging dislocation line bends along the shape of the SFT during the interaction. Due to dislocation line bending, the character of dislocation segment on an SFT inevitably changes because the dislocation's character is given by the orientation relationship between Burgers vector and the line sense. The variation of dislocation character upon interaction with an SFT for screw, 60° mixed, and edge dislocations are summarized in Fig. 9. The bending manner of a dislocation on two different but crystallographically equivalent SFTs is dependent on the SFT geometry. As a result of the difference in bending manner, the dislocation line segments on the two different SFTs inevitably become different in character. Assuming the character of the segment on the SFT is a 60° mixed dislocation in Fig. 3(a), the character of the segment inevitably becomes screw in Fig. 3(b). These results are the evidence that the Burgers vector of dislocation line segments on the SFT is a key factor determining which type of SFT destruction process is induced. Strictly speaking, Type 1 and Type 2

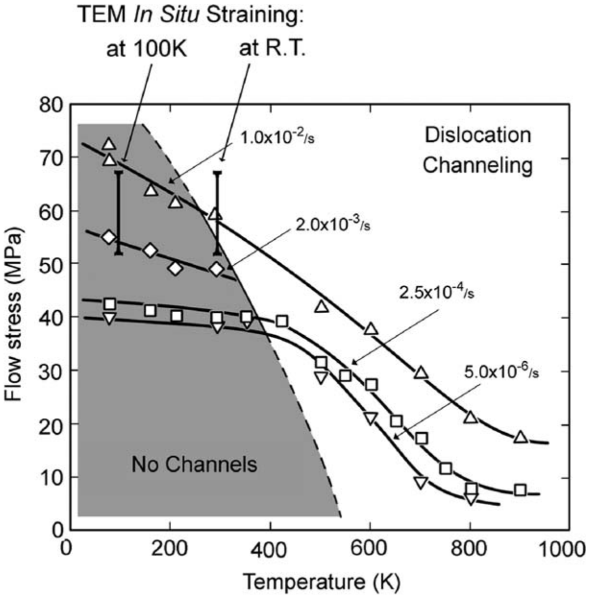

Fig. 8. Temperature dependence of dislocation channeling in quenched gold containing large SFTs (≈50 nm), reported by Yoshida et al. [12]. The present TEM in situ straining at room temperature is located in the range of cleared channel formation in Yoshida's experiments, whereas in situ straining at 100 K is located in the range of no channel formation.

processes are slightly inconsistent with Kimura's models. For instance, in Fig. 1 a triangular Frank loop was apparently formed on the plane parallel to the dislocation glide plane, whereas in the Kimura model for 60° mixed dislocation a Frank loop is formed on a {1 1 1} plane that is not parallel to the dislocation glide plane, as shown in Fig. 10. The details of Kimura's models may need to be revised; however, the agreement in the major features of SFT destruction strongly indicates that these destruction processes were induced by dislocation reactions similar to Kimura models.

The Type 3 process does not fit Kimura's models, because none of his models leave a small SFT after SFT collapse. The details of this process, e.g. how the Burgers vector of the dislocation affects the process, still remain unclear. However, it was found that at least one of two variants of this process is accompanied by vacancy transport and re-clustering. Assuming that vacancy migration is a key physical attribute of the Type 3 process, this process would be sensitive to temperature. As seen in Fig. 6, an aggregate of vacancies was formed on the gliding dislocation, indicating that the vacancy transport in the Type 3 process occurred via mechanisms similar to dislocation pipe diffusion. Ballufi estimated the activation energy of self-diffusion via dislocation pipe diffusion in pure copper as 1.53 eV [21], which is significantly smaller than the energy via ordinary lattice diffusion given as 2.01 eV (vacancy formation energy: 1.27 eV plus migration energy: 0.74 eV) [22]. Supposing the pipe diffusion is the vacancy transport mechanism, it is highly possible that the Type 3 process can occur at temperatures much lower than room temperature. Moreover, an alternative to the pipe diffusion mechanism was recently observed in MD simulations. A significant number of vacancies can be transported to the specimen surfaces via multiple

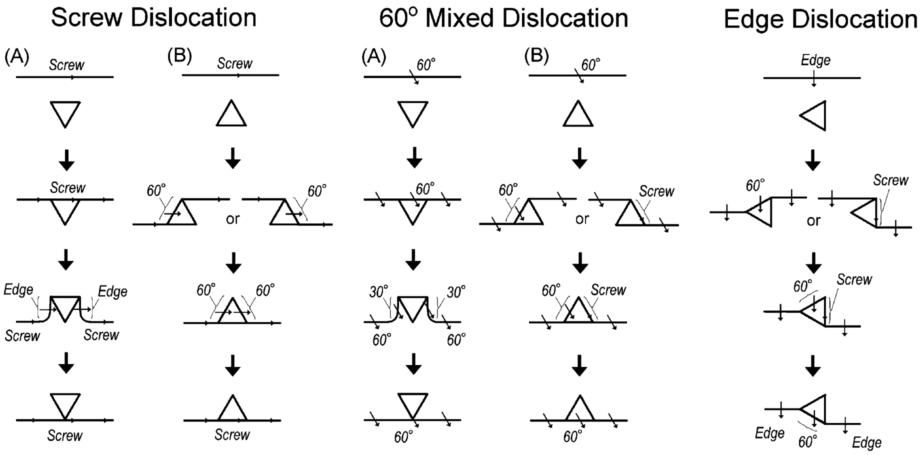

Fig. 9. Variation of dislocation type accompanied with bending of dislocation line on an SFT. Two types of SFT-dislocation configurations correspond to two types of SFTs crystallographically equivalent each other. When a gliding dislocation interacts these two crystallographically equivalent two SFTs, line segments on each SFTs inevitably become different character.

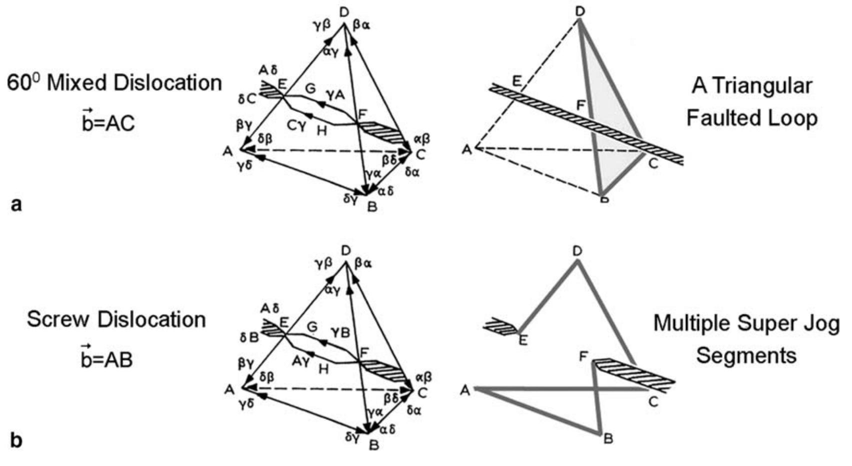

Fig. 10. Kimura's SFT collapse models induced by direct interaction with (a) a 60°mixed dislocation and (b) a screw dislocation [20].

dislocation cross-slip [23]. This mechanism is rather fast and weak temperature dependent.

To date, the Type 1 and 2 SFT collapse processes have not been reproduced in MD simulations, whereas a process similar to the Type 3 has been observed [23]. A conceivable factor for this inconsistency may be the size of SFTs. The maximum SFT size simulated with MD codes to date is about 12 nm [23], which is in the stable size range where the SFT is energetically more stable than a Frank loop, whereas the SFT size of the present study is in the meta-stable size range where the SFT would prefer to transform into a Frank loop [17]. More simulation, theory, and in situ TEM experiments are needed to resolve this issue.

The role of these three SFT destruction process for cleared channel formation is still unclear. The Type 3 process does not annihilate the whole SFT. In this respect the Type 3 process is less efficient for annihilating an SFT. It is also true that obstacles to subsequent gliding dislocations also remain for the other two processes. For instance, although the Type 2 process does not leave remnants after the SFT annihilation, the super jog segments formed on the screw dislocations which are responsible for this destruction process are sessile. These sessile segments on screw dislocations following the Type 2 process would become an obstacle for its own and subsequent gliding dislocations. The remnant of Type 1, a faulted triangle loop, is a two-dimensional defect cluster, which does not disturb subsequent dislocations gliding on other (1 1 1) planes parallel to the Frank loop. In this respect, Frank loops are less harmful obstacles than small SFTs remaining after the Type 3 process. Because Frank loops are 2-D clusters, the chance of annihilating the Frank loop may be less than the chance of annihilating small SFTs that are 3-D clusters. In order to resolve the influence of each defect annihilation process on cleared channel formation, we need to identify the role of each type of remnant. Also, further investigation is necessary to identify the factors which control the competition between the SFT destruction processes.

Acknowledgments

This research was sponsored by Office of Fusion Energy Sciences, US Department of Energy, under contract DE-ACO5-00OR22725 with UT-Battelle, LLC. We are grateful to Ms Kathy Yarborough for specimen preparation, Mr Cecil Carmichael for furnace operation for heat treatments, and Dr Neal Evans for maintenance of TEM. The authors also thank Dr B.N. Singh, Risø National Laboratory, for valuable discussions and comments.

References

[1] J.V. Sharp, Philos. Mag. 16 (1967) 77.
[2] A. Okada, K. Kanao, T. Yoshiie, S. Kojima, Mater. Trans., JIM 30 (4) (1989) 265.
[3] K. Farrell, T.S. Byun, N. Hashimoto, J. Nucl. Mater. 329–333 (2004) 471.
[4] R.P. Tucker, M.S. Wechsler, S.M. Ohr, J. Appl. Phys. 40 (1969) 400.
[5] L.M. Howe, Rad. Effect Defect Solid 23 (1974) 181.
[6] T. Diaz de la Rubia, H.M. Zbib, T.A. Khraishi, B.D. Wirth, M. Victoria, M.J. Caturla, Nature 406 (2000) 871.
[7] M. Kiritani, Mater. Chem. & Phys. 50 (1997) 133.
[8] S.J. Zinkle, L.L. Snead, J. Nucl. Mater. 225 (1995) 123.

[9] M. Victoria, N. Baluc, C. Baliat, Y. Dai, M.I. Luppo, R. Schaublin, B.N. Singh, J. Nucl. Mater. 276 (2000) 114.

[10] Yu.N. Osetsky, D.J. Bacon, B.N. Singh, B.D. Wirth, J. Nucl. Mater. 307–311 (2002) 852.

[11] M.S. Bapna, T. Mori, M. Meshii, Philos. Mag. 17 (1968) 177.

[12] S. Yoshida, M. Kiritani, Y. Deguchi, N. Kamigaki, Mat. Trans. JIM 9 (Suppl.) (1968) 83.

[13] T. Mori, M. Meshii, Acta Met. 17 (1969) 167.

[14] A. Yoshinaka, Y. Shimorura, M. Kiritani, S. Yoshida, Jpn. J. Appl. Phys. 7 (1968) 709.

[15] J. Silcox, P.B. Hirsch, Phil. Mag. 4 (1959) 72.

[16] Y. Matsukawa, S.J. Zinkle, J. Nucl. Mater. 329–333 (2004) 919.

[17] T. Jøssang, J.P. Hirth, Phil. Mag. 13 (1966) 657.

[18] B.D. Wirth, V.V. Bulatov, T. Diaz de la Rubia, J. Eng. Mat. Tech. 124 (2002) 329.

[19] Yu.N. Osetsky, R.E. Stoller, Y. Matsukawa, J. Nucl. Mater. 329–333 (2004) 1228.

[20] H. Kimura, R. Maddin, Lattice defects in quenched metals, in: R.M.J. Cotterill (Ed.), Proceedings of an International Conference, Argonne National Labratory, June 15–17, 1964, Academic Press, New York, 1965, p. 319.

[21] R.W. Balluffi, Phys. Stat. Solid 42 (1970) 11.

[22] P.R. Bourassa, B. Lengeler, J. Phys. F: Met. Phys. 6 (1976) 1405.

[23] Yu.N. Osetsky, Y. Matsukawa, R.E. Stoller, S.J. Zinkle, Phys. Rev. Lett., submitted for publication.